Global Analysis of Oceanographic Data

Sydney Levitus and Abraham H. Oort
Geophysical Fluid Dynamics
Laboratory/NOAA
Princeton University
Princeton, N.J. 08540

Abstract

A project to objectively analyze a large quantity of oceanographic data for the world ocean is described. Preliminary results are encouraging within the limits of data available. Results are being used in a variety of ways but at present primarily for studies of the ocean's role in the global heat balance. A brief discussion of the data used, the method of analysis, and some preliminary results is presented.

1. Introduction

The study of the global climate requires a knowledge of the physical structure of the world ocean. The Observational Studies Group at the Geophysics Fluid Dynamics Laboratory/NOAA is using all available temperature, salinity, sigma-t, and oxygen data for the world ocean on file at the National Oceanographic Data Center (NODC), Washington, D.C., to construct the global fields of these data on a 1° latitude-longitude grid at standard oceanographic analysis levels between the surface and 5000 m depth. The analysis of temperature was carried out using Nansen cast data, mechanical bathythermograph (MBT) data, and expendable bathythermograph (XBT) data, which together form a data set of ~1 200 000 soundings. Preliminary results from the project appear in papers by Oort and Vonder Haar (1976) and Ellis *et al.* (1977). These papers deal with hemispheric and global heat balances that should be of particular interest to researchers in the fields of large-scale air-sea interaction, physical oceanography, and climatology. The purpose of this paper is to discuss the data used and their distribution, the method of analysis, and problems encountered in carrying out an automated analysis of oceanographic data. Sections and charts are shown that can be directly compared to earlier results based on more limited data. In addition, a few examples are shown of new sections that can be derived from the analyzed data.

2. Data and data distribution

The data used in this project were obtained from NODC, Washington, D.C., and represent all historical data available through June 1973. The distribution with depth of the total number of observations for temperature, salinity, and oxygen and of the number of 1° squares containing observations of these parameters is summarized in Table 1. Also given in Table 1 as a function of depth is the number of 1° squares over the globe that contain ocean.

The Oceanographic Station Data (SD) file contained ~400 000 hydrographic stations and consisted primarily of Nansen cast data of temperature, salinity, sigma-t, and oxygen but also contained several thousand salinity-temperature-depth (STD) casts. The distribution of the number of temperature observations in this file as a function of depth for the globe and for individual hemispheres is shown in Fig. 1a.

The MBT file contained ~740 000 soundings of which ~100 000 were from weather ship stations. The maximum observation depth for the MBT soundings is 295 m, so that the deepest standard level for which MBT data are available is 250 m. The distribution of the number of MBT observations as a function of depth for the globe and for individual hemispheres is shown in Fig. 1b.

Finally, the XBT file contained ~100 000 stations, the majority of which were shipboard XBTs (SXBTs) but there were also ~3300 aircraft XBTs (AXBTs). The AXBTs were not included in this study because they were not as accurate as the SXBTs. Future references to the XBT file in this article refer only to SXBT measurements. The maximum depth that we encountered for any of the XBT soundings was 1830 m, but only observations shallower than 1000 m were used. The distribution of the number of XBT observations as a function of depth for the globe and for individual hemispheres is shown in Fig. 1c. Both the SD and the MBT file obtained from NODC contained data that NODC had interpolated from the original soundings to standard levels. The XBT data were not interpolated to standard levels by NODC, so we linearly interpolated the profiles to standard levels. Additional information concerning the data can be found in the *User's Guide to NODC's Data Services* (NOAA, 1974).

The global distributions of 1° squares containing temperature observations at the sea surface for the SD, MBT, and XBT files, separately and for the merged sum of all three files, are shown in Figs. 2–5, respectively, for the annual period. The designation "annual period" refers to the fact that all observations in each file are included regardless of the time or date of measurement. The figures show a bias in the distribution of observations toward Northern Hemisphere coastal regions. The distribution of MBT and XBT observations in Figs. 3 and 4 clearly indicates great circle routes taken by ships. These patterns suggest that the soundings may have been "measurements of opportunity" since XBTs and MBTs can be lowered while a ship is in motion.

To show the seasonal distribution of the observations, we present 2 months that are more or less typical for the winter and summer seasons. The distribution of the

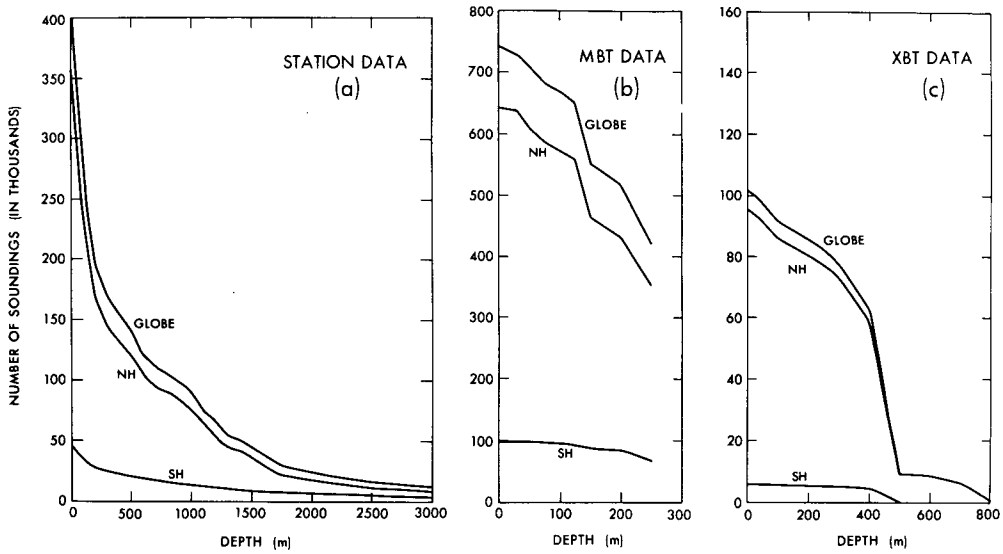

FIG. 1. Distribution of (a) SD temperature observations, (b) MBT observations, and (c) XBT observations as a function of depth for the globe and the Northern and the Southern Hemisphere.

TABLE 1. Distribution with depth of the number of 1° squares of ocean (Ocean ODSQS); the total number (N) of temperature, salinity, and oxygen observations; and the number of 1° squares (ODSQS) containing observations of each of these parameters.

Standard Level	Depth, m	Ocean ODSQS	Temperature		Salinity		Dissolved Oxygen	
			N	ODSQS	N	ODSQS	N	ODSQS
1	0	42 311	1 215 157	30 538	370 406	21 239	131 752	17 350
2	10	42 208	1 200 680	30 606	364 980	21 182	137 829	17 867
3	20	42 052	1 188 222	30 575	356 208	21 122	135 870	17 851
4	30	41 915	1 166 344	30 516	343 131	21 022	133 380	17 804
5	50	41 331	1 123 666	30 302	318 416	20 695	127 537	17 577
6	75	41 021	1 063 936	29 949	283 791	20 267	115 883	17 154
7	100	40 390	1 020 579	29 729	258 888	20 002	107 817	16 932
8	125	40 230	968 922	29 508	228 171	19 711	99 951	16 711
9	150	39 917	855 879	29 193	214 788	19 541	95 823	16 476
10	200	39 305	790 633	28 760	186 358	19 191	89 112	16 169
11	250	39 105	677 113	27 458	172 123	18 943	83 893	15 940
12	300	38 670	245 905	20 817	162 228	18 270	79 925	15 676
13	400	38 314	216 612	20 157	147 570	18 214	74 550	15 284
14	500	37 885	150 677	18 350	135 176	17 710	68 330	14 880
15	600	37 385	129 810	17 838	115 861	17 228	59 130	14 601
16	700	37 385	117 184	17 433	106 467	16 941	55 106	14 438
17	800	37 089	106 313	16 985	101 489	16 724	52 324	14 168
18	900	36 908	99 367	16 697	94 724	16 413	49 697	13 973
19	1000	36 518	90 482	16 188	86.346	15 895	45 377	13 415
20	1100	36 339	75 416	15 264	71 418	14 930	39 445	12 796
21	1200	36 081	66 676	14 523	63 765	14 188	33 582	11 992
22	1300	35 887	55 811	13 699	53 376	13 359	29 900	11 493
23	1400	35 739	51 564	13 286	49 334	12 953	27 801	11 106
24	1500	35 427	44 878	12 742	42 910	12 470	24 510	10 469
25	1750	34 933	30 206	11 253	28 803	10 966	20 156	9 468
26	2000	33 870	24 814	10 075	23 624	9 792	16 546	8 396
27	2500	32 081	17 638	8 229	16 804	7 963	12 083	6 948
28	3000	29 191	12 870	6 681	12 260	6 438	8 963	5 643
29*	3500	25 091	5 312	3 251	4 862	3 028	4 000	2 751
30	4000	19 720	6 382	3 581	6 043	3 408	4 523	2 934
31*	4500	12 858	1 679	1 101	1 540	1 033	1 182	875
32	5000	6 884	1 628	1 045	1 479	971	1 074	794

* These levels are not standard NODC levels. The data presented are interpolations from standard levels above and below the respective level.

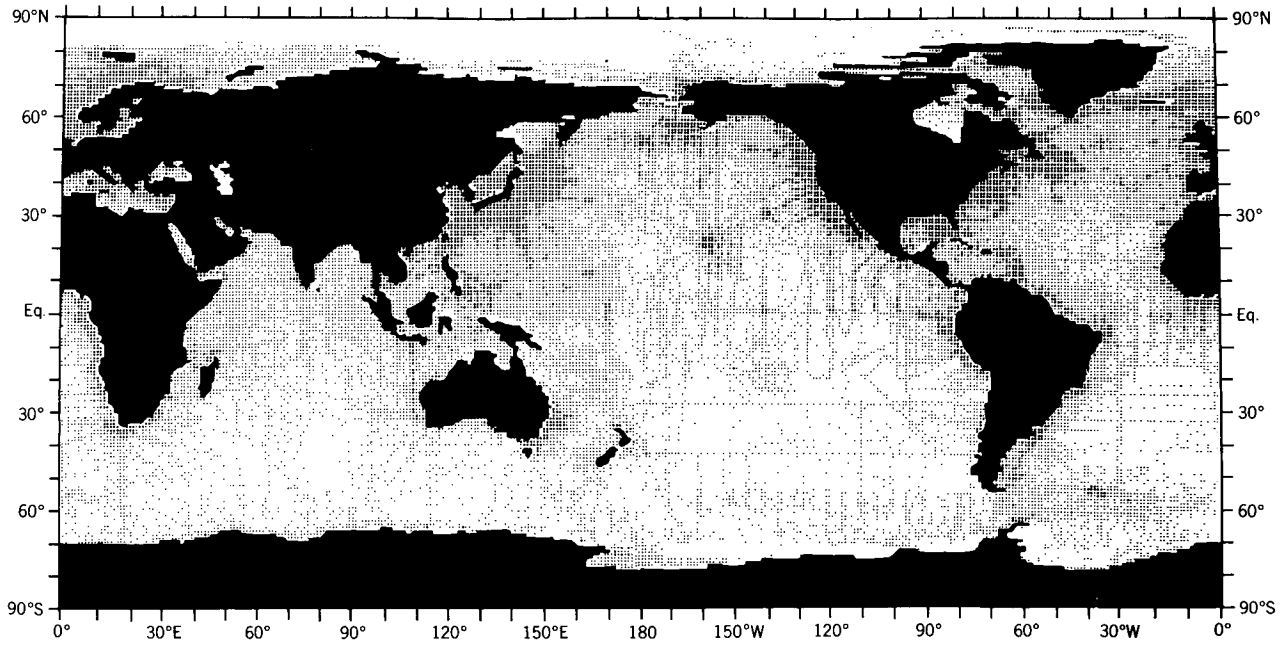

FIG. 2. Sea surface distribution of 1° squares containing SD temperature observations for the annual period. A small dot indicates a square containing 1–9 observations, and a large dot indicates 10 or more observations.

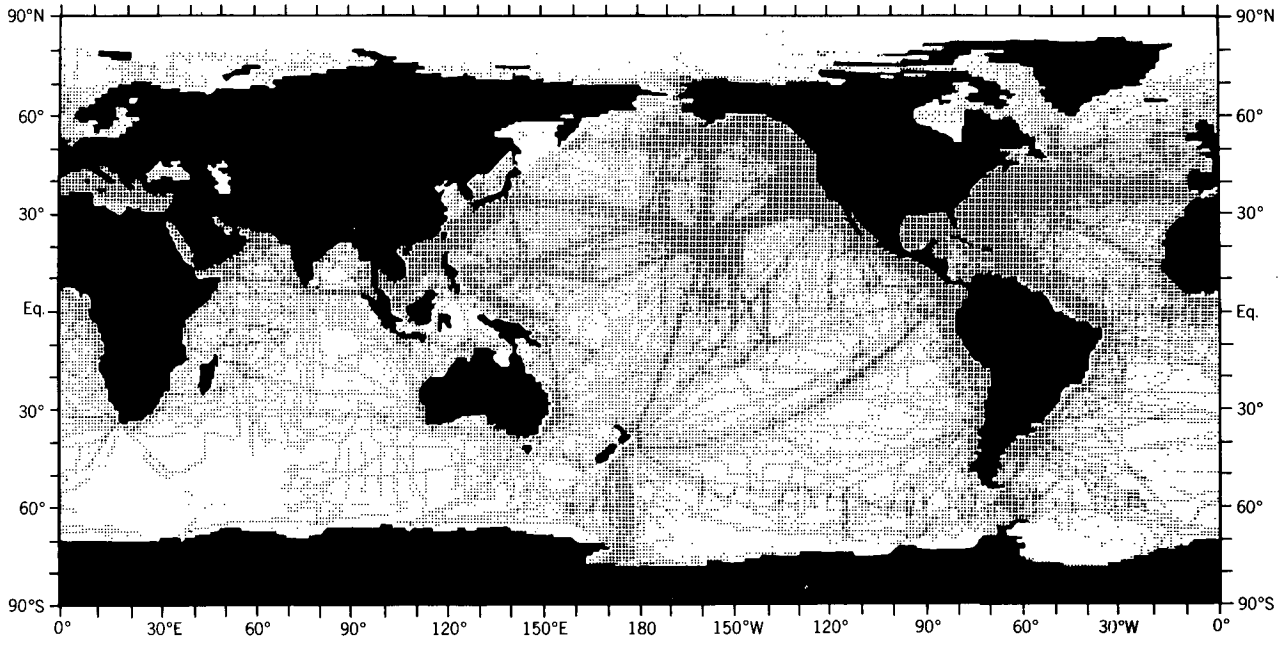

FIG. 3. Sea surface distribution of 1° squares containing MBT observations for the annual period. A small dot indicates a square containing 1–9 observations, and a large dot indicates 10 or more observations.

merged temperature observations at the sea surface for the selected months of March and September, regardless of year, are shown in Figs. 6 and 7, respectively. These figures show clearly the relative paucity of Southern Hemisphere data. In order to produce monthly temperature analyses, it is clear that all available data consisting of Nansen cast, MBT, and XBT soundings had to be used.

The question of the propriety of merging the three types of temperature observations will be discussed now. The accuracy of the SD measurements is ~0.01°C. However, for the MBT and XBT measurements it is much less, probably of the order of a few tenths of a degree. Averaging of the data in 1° squares, diurnal temperature variations, the march of the annual temperature wave within a monthly averaging period, and the existence

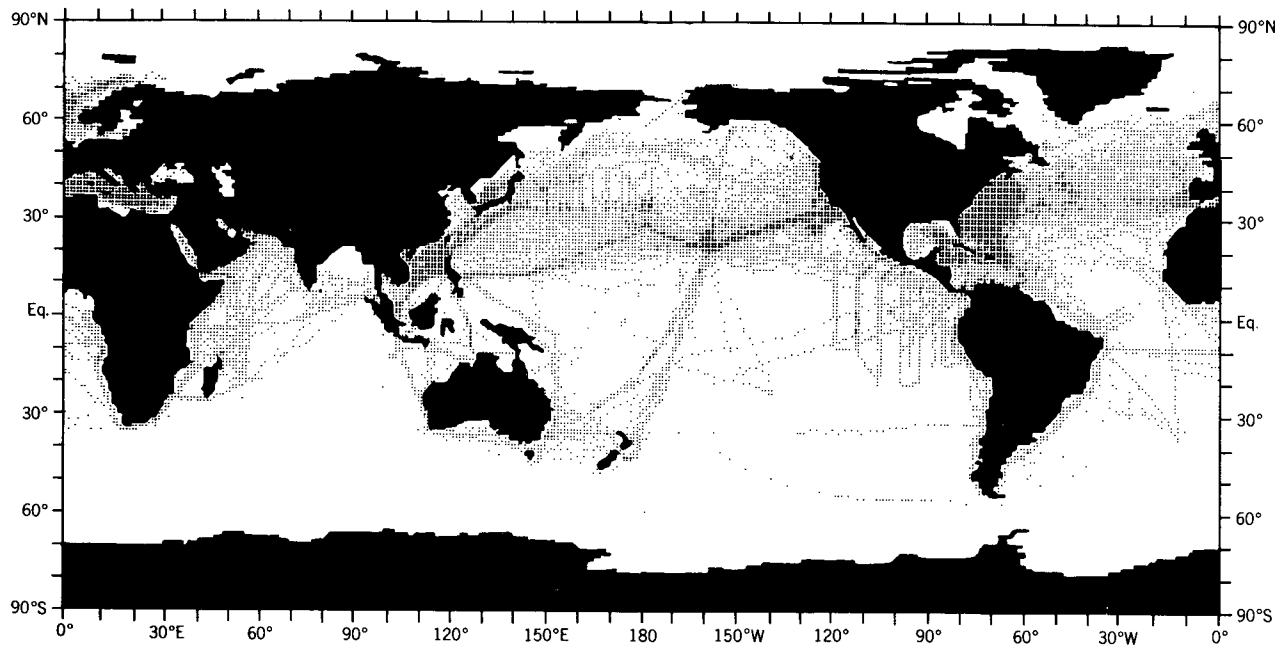

FIG. 4. Sea surface distribution of 1° squares containing XBT observations for the annual period. A small dot indicates a square containing 1–9 observations, and a large dot indicates 10 or more observations.

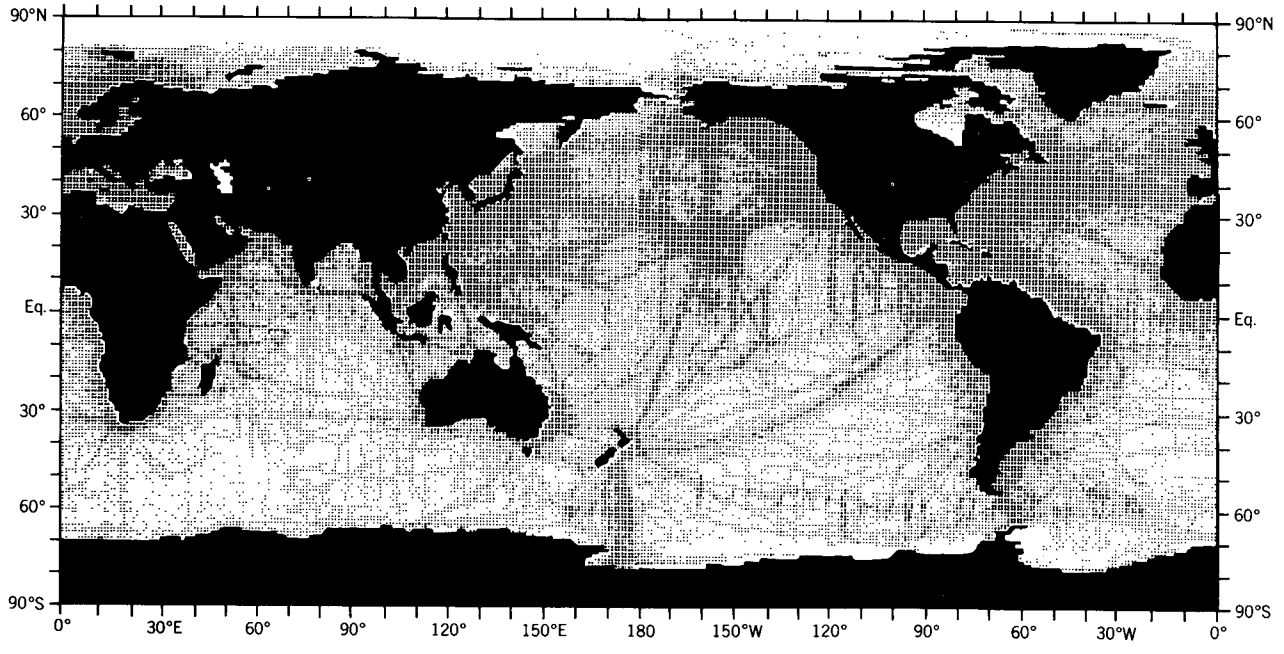

FIG. 5. Sea surface distribution of 1° squares containing observations from the merged data set consisting of all SD, MBT, and XBT temperature observations for the annual period. A small dot indicates a square containing 1–9 observations, and a large dot indicates 10 or more observations.

of mesoscale eddies and internal waves in the ocean all contribute to an uncertainty that can be larger than the difference in accuracy of the instruments in the upper layer of the ocean. For these reasons, we have used all historical data available. To show a comparison of the measurements by different instruments, we have prepared Table 2, which presents the number of observations, the mean, and the standard deviation of the three types of measurements for selected Marsden squares. The comparison is given for the 250 m level in order to minimize the standard deviation due to temperature changes resulting from the annual march of temperature. Marsden squares in the mid-Pacific Ocean were chosen in order to minimize contributions from water

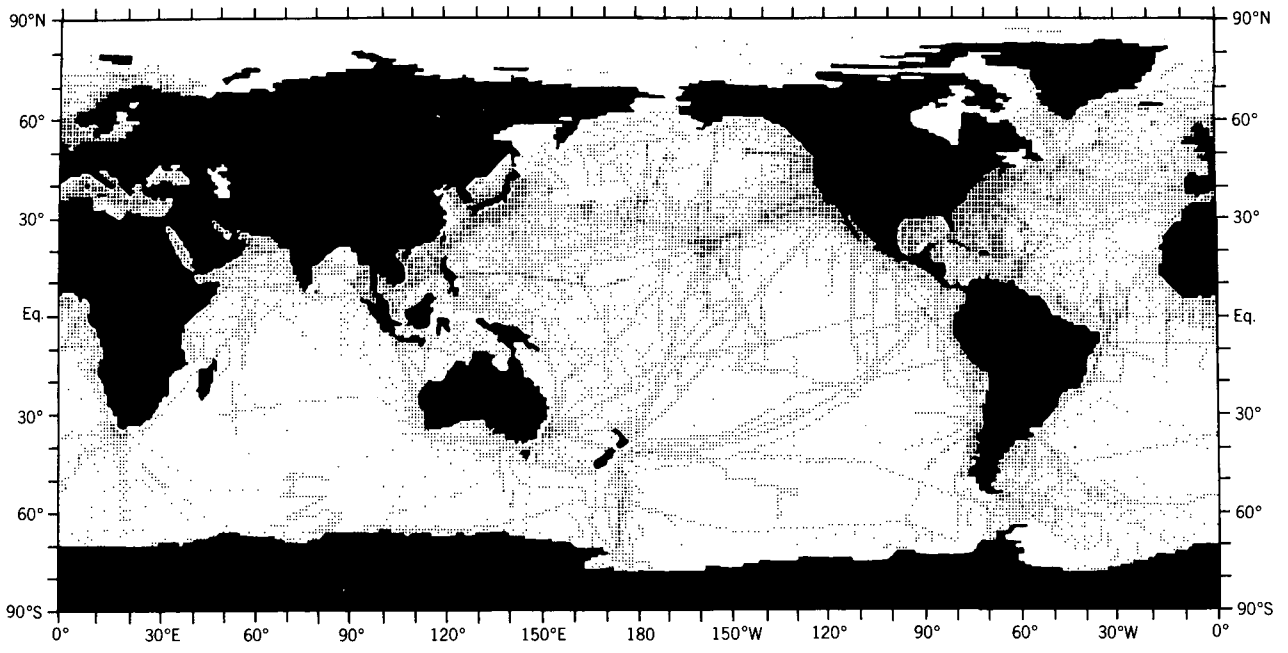

FIG. 6. Sea surface distribution of 1° squares containing temperature observations from the merged temperature data set for the month of March. A small dot indicates a 1° square containing 1–4 observations, and a large dot indicates 5 or more observations.

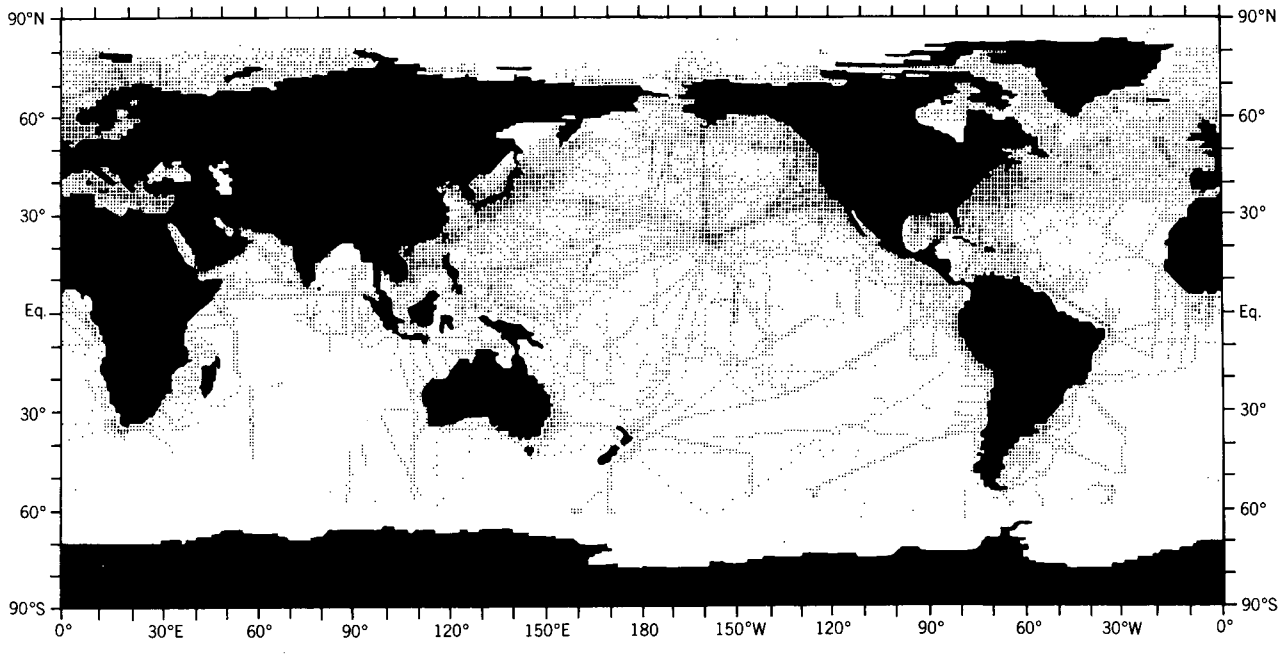

FIG. 7. Sea surface distribution of 1° squares containing temperature observations from the merged temperature data set for the month of September. A small dot indicates a 1° square containing 1–4 observations, and a large dot indicates 5 or more observations.

masses of widely different properties, which one would expect to find in coastal areas. Although we are comparing measurements from large areas and the data are far from being synoptic, the measurements agree to within 1 standard deviation. Examination of the results for other Marsden squares (which are not given here) also shows similar agreement, with some exceptions in western boundary current regions.

As a further example, the April distribution of 1° squares containing salinity observations from the SD file is shown in Fig. 8. Large areas of the Southern Hemisphere are totally devoid of observations, and there are fairly large void regions in the Northern Hemisphere as well. Maps of the distribution of salinity

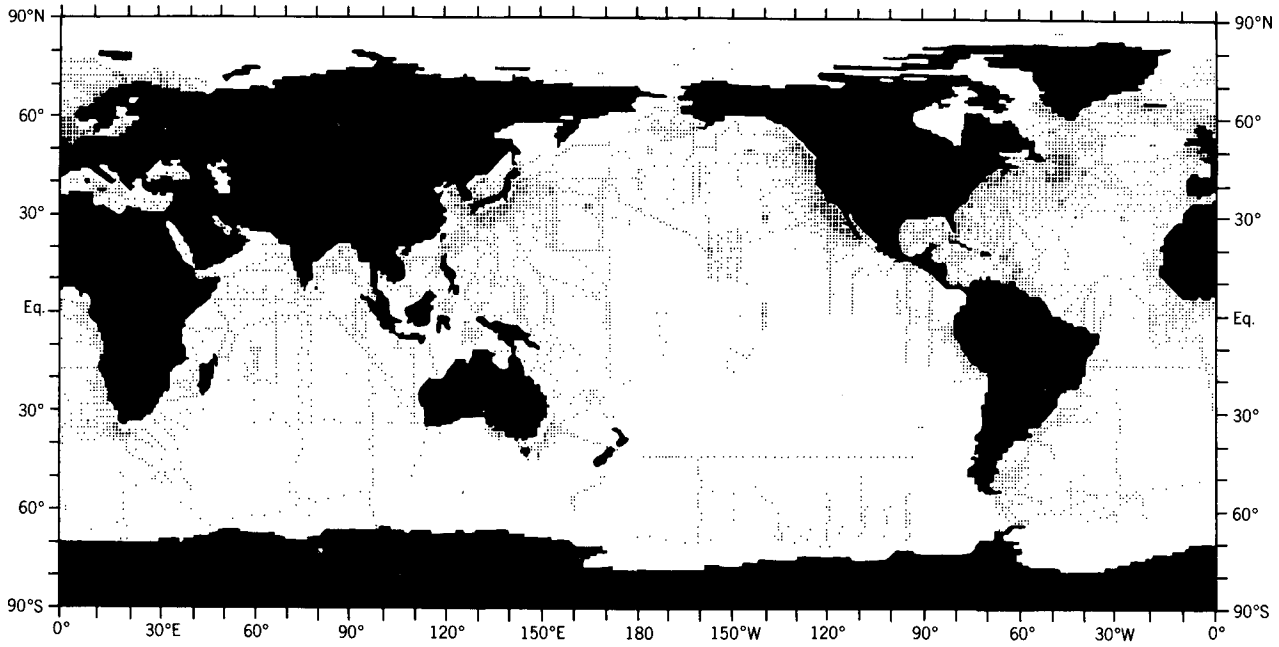

FIG. 8. Sea surface distribution of 1° squares containing salinity observations for the month of April. A small dot indicates a square containing 1–4 observations, and a large dot indicates 5 or more observations.

observations for other months and for all standard levels from the sea surface to a depth of 1000 m show a similar geographical bias. An interesting feature of these maps is that they clearly show the cruise tracks of various expeditions; for example, the cruise track at 43°S (Fig. 8) is from observations taken by the Scorpio Expedition.

The distribution of observations of dissolved oxygen at the sea surface for the annual period is shown in Fig. 9. There are only about one-tenth as many observations of oxygen as compared to temperature. However, the distribution is fairly uniform and allowed us to produce a global analysis for the annual period. Although the number of observations of oxygen decreases with depth, their geographical distribution remains fairly uniform at all levels.

3. Data reduction and quality control

Although the great majority of observations were found to be acceptable, the major problem we have encountered in this project has been quality control of the data. The relatively few observations that are greatly in error can easily be eliminated by checking whether

TABLE 2. A comparison for the annual case of the three types of temperature measurements used.

		Station Data			MBT			XBT		
Latitude	MSQ	N	$\bar{T}$	$(\overline{T'^2})^{\frac{1}{2}}$	N	$\bar{T}$	$(\overline{T'^2})^{\frac{1}{2}}$	N	$\bar{T}$	$(\overline{T'^2})^{\frac{1}{2}}$
50°–60°N	198	1179	3.8	0.3	1994	4.0	0.6	68	4.3	1.2
40°–50°N	162	463	5.5	1.9	2684	5.7	2.7	60	6.2	1.5
30°–40°N	126	85	12.2	1.6	1055	12.1	1.7	359	12.6	1.0
20°–30°N	90	67	15.0	1.0	2210	14.9	1.1	549	14.8	1.0
10°–20°N	54	43	12.4	2.3	784	13.5	2.7	32	14.5	1.9
0°–10°N	18	83	11.2	1.4	486	10.9	1.9	4	9.6	0.1
0°–10°S	317	80	14.6	2.3	249	14.9	2.3	75	17.0	2.6
10°–20°S	353	49	19.1	1.0	465	19.2	1.0	137	19.7	0.8
20°–30°S	389	34	16.6	1.8	404	17.0	1.8	72	16.8	1.4
30°–40°S	425	23	13.2	1.1	510	12.7	1.2	27	13.4	1.0
40°–50°S	461	33	9.9	1.9	550	10.4	1.6	1	13.6	0.0
50°–60°S	497	16	5.0	1.6	100	4.8	2.0	—	—	—
60°–70°S	533	22	1.3	0.2	125	1.2	0.6	—	—	—

For each Marsden square (MSQ) the number of observations (N), the mean temperature ($\bar{T}$), and the standard deviation of the temperature $(\overline{T'^2})^{\frac{1}{2}}$ at the 250 m level are given for each type of measurement. All the Marsden squares listed lie in the meridional belt 170°–180°W.

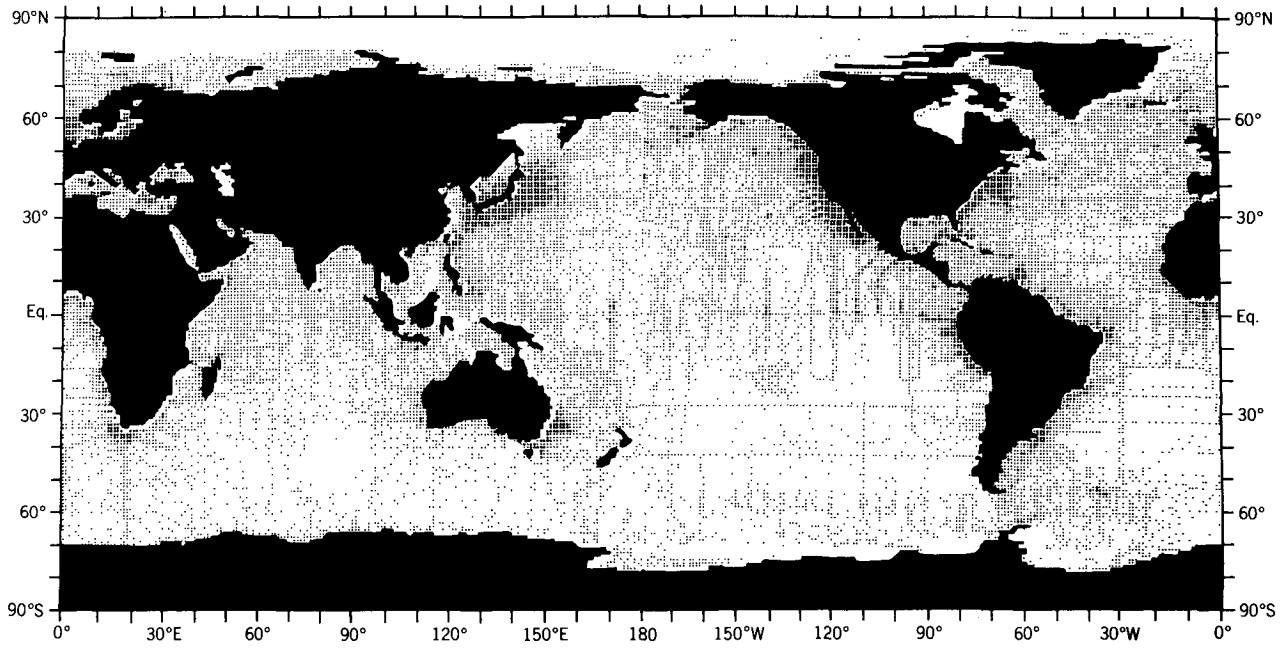

FIG. 9. Sea surface distribution of 1° squares containing dissolved oxygen observations for the annual period. A small dot indicates a square containing 1–9 observations, and a large dot indicates 10 or more observations.

or not each observation falls within a reasonable range. However, this kind of checking can only be used for gross error checks, since if the range is too restrictive, one would eliminate good data.

In the actual procedure, range checking was only done on the data in the MBT and XBT files, with an allowable range of temperatures between −7°C and 35°C. An additional and more important error check that was performed on all the data is described as follows. All data for each parameter and at each standard analysis level were averaged by Marsden square (10° square) to produce a record of the number of observations, the mean value, and the standard deviation in each square. A final data set was then produced by eliminating all observations in the Marsden square that differed from the mean by more than 5 standard deviations. In general, <0.5% of all observations were eliminated. Marsden squares containing <4 observations were not checked in this way, and the data were accepted as reported. After the final analysis of the various fields, we have still found obviously incorrect data, which were responsible for a poor analysis in the vicinity of these data points. There are many Marsden squares and even 1° squares for which the spatial variations and the annual and interannual differences are quite large. For example, squares that include coastal areas may exhibit an extremely large salinity variation due to an annual variation in river runoff. Squares may encompass areas occupied at different times by water masses with quite different properties, a situation that could arise due to the meandering of an ocean current such as the Gulf Stream.

Quality control of oceanographic data becomes more critical at greater depths. This is because of the relatively small gradients of oceanographic fields at large depth and the lack of a sufficient number of observations upon which to build strict quality control standards. Even errors on the order of 0.1°C in temperature, 0.03‰ in salinity, and 0.1 ml/l in oxygen will adversely effect the analyses of these parameters in the deep ocean. It is for this reason that XBT observations were not used below 1000 m. An example of possible errors in the analyses of the deep ocean will be given in a later section of this paper.

Another possible source of problems that had to be considered was positional errors in the reports. If the error in location is such that the sounding is placed in the wrong Marsden square, then, depending on the number of observations and the differences between the value of the erroneous sounding and the correctly located soundings, the erroneous sounding may or may not be eliminated through our error checking. An error in location such that an observation is placed in a 1° square defined as land, resulted in the observation not being used in the analysis.

Ocean depths for each 1° square on the globe were based on the report by Smith *et al.* (1966). In regions poleward of 49° latitude, their topography was based on regions larger than 1° squares, so that an interpolation had to be performed to produce a 1° square topography for this region. Smith *et al.* discussed the methods used in determining ocean depths and possible sources of error. It was necessary to use a land-sea table for defining the "ocean" basins because position errors placed some soundings in land areas.

4. Representativeness of the data

Another problem that arises in conjunction with quality control is the representativeness of the data. The general paucity of data forces us to use all historical data. This implies that in any given 1° square there may be data from a month or season of one particular year while in the same or a nearby square there may be data from an entirely different year. If there is a large interannual variability in a region where scattered sampling in time has occurred, then one can expect the analysis to reflect this. Because the observations are scattered with respect to time, except for a few limited areas, the results cannot in a strict sense be considered a true long-term climatological average. What we have attempted to produce for each parameter with the presently available data are analyses of the monthly, seasonal, and annual fields that show the dominant variations in the large-scale permanent or semipermanent features of the field.

Another possible source of bias may arise because sometimes measurements have intentionally been taken in an area experiencing anomalous conditions. An example of this would be the repeated sampling of certain warm or cold eddies. We have not investigated this possible bias specifically and mention it only to illustrate another, but probably less significant, source of error in an analysis project of this type.

5. Method of analysis

An objective analysis scheme of the iterative difference-correction type (Cressman, 1959) was used to analyze the data. Inputs to the analysis scheme were the observed 1° square means of data for whatever period was being analyzed and a first guess value for each square. For instance, the 1° square means for our annual analysis were computed using all available data regardless of the date of observation. If we were computing an analysis of temperature for the month of July, we used all the historical July data.

The analysis scheme for any analysis level works as follows. Each 1° square value is defined as being representative of the center of that particular 1° square. The 360 × 180 grid points are located at the intersection of ½° lines of latitude and longitude. The average distance between data points (1° squares containing observed means) on the analysis level is computed by taking the square root of the total ocean area divided by the number of data points. An influence radius is now defined as a multiple of the average distance between observation points. At those grid points where there is an observed mean value, the difference between the mean and the first guess field is computed. A correction to the first guess value at all grid points is then computed as a distance weighted mean of all grid point difference values that lie within the area around the grid point defined by the influence radius. Mathematically, the correction factor is given by the expression,

$$C_{i,j} = \sum_{s=1}^{n} W_s Q_s / \sum_{s=1}^{n} W_s, \tag{1}$$

where,

$C_{i,j}$ the correction factor at point (i, j);
i, j coordinates of a grid point in the east–west and north–south directions, respectively;
n the number of observations that fall within the area around the point i, j defined by the influence radius;
Q_s the difference between the first guess and the observed mean at the sth point in the influence area;
$W_s = \exp(-Er^2R^{-2})$, for $r \leq R$;
$W_s = 0$, for $r > R$;
r distance of the observation from the grid point;
R influence radius;
$E = 4$.

The derivation of the weight function, W_s, will be presented later in this section. At each grid point we compute an analyzed value, $G_{i,j}$, as the sum of the first guess, $F_{i,j}$, and the correction, $C_{i,j}$, at the point. The expression for this is simply

$$G_{i,j} = F_{i,j} + C_{i,j}. \tag{2}$$

If there are no data points within the area defined by the influence radius, then the correction is zero, the first guess field is left unchanged, and the analyzed value is simply the first guess value. Another gross error check is used at this point in the analysis scheme. If the absolute magnitude of the difference Q_s at any grid point exceeds some prescribed limit, which is a constant for the entire analysis level, then the correction is not used. This correction procedure is followed at all grid points to produce an analyzed field. This field is then used as the new first guess field, and the procedure is repeated until the analysis shows little change. The number of iterations required depends on the disparity between the first guess field and the observed input data. The smaller the difference, the fewer the iterations that are required. After each iteration, the resulting field was smoothed with a Laplacian smoother.

The analysis scheme is set up so that the influence radius, the error limit for the correction factor, the number of smoothings, and the intensity of smoothing can be varied with each iteration. The strategy used is to begin the analysis with a large influence radius and decrease it with each iteration. This technique allows us to analyze progressively smaller-scale phenomena with each iteration.

The analysis scheme is based on the work of several researchers whose efforts were directed toward the analysis of meteorological data. Bergthörsson and Döös (1955) computed corrections to a first guess field using various techniques. One of these techniques was to assume that the difference between a first guess value and an analyzed value at a grid point was the same as the difference at an observing station. All the observed differences in an area surrounding the grid point were then averaged and added to the grid point first guess value to produce an analyzed value. Cressman (1959) modified this method by applying a distance-related weight function to each

observation used in the correction in order to give more weight to observations that occur closest to the grid point. In addition, Cressman introduced the method of performing several iterations of the analysis scheme using the analysis produced in each iteration as the first guess field for the next iteration. He also suggested beginning the analysis with a relatively large influence radius and decreasing it with successive iterations so as to analyze smaller-scale phenomena with each pass.

Sasaki (1960) introduced a weight function that was specifically related to the density of observations. Barnes (1963) extended the work of Sasaki, and it is the weight function presented by Barnes that has been used in our analysis. The derivation of the weight function, which we present for completeness, follows the work of Sasaki and Barnes.

The principle upon which the weight function was derived was given succinctly by Barnes (1963, p. 2) and is that "the two-dimensional distribution of an atmospheric variable can be represented by the summation of an infinite number of independent harmonic waves, that is, by a Fourier integral representation." If $f(x, y)$ is the variable to be represented, then in polar coordinates r, θ a smoothed or filtered function, $g(x, y)$, can be defined as follows:

$$g(x, y) = \frac{1}{2\pi}\int_0^{2\pi}\int_0^{\infty} \eta f(x + r\cos\theta, y + r\sin\theta) \times d(r^2/4K)d\theta, \quad (3)$$

where r is the radial distance from a grid point whose coordinates are x, y. The weight function, η, is defined as $\eta = \exp(-r^2/4K)$, which resembles the Gaussian distribution in form. The exact shape of the weight function is determined by the value of K, which is dependent on the distribution of data. The determination of K follows.

The weight function has the property that

$$\frac{1}{2\pi}\int_0^{2\pi}\int_0^{\infty} \eta d(r^2/4K)d\theta = 1. \quad (4)$$

This property is desirable because in the continuous case (3) the application of the weight function to the distribution $f(x, y)$ will not change the mean of the distribution. However, in the discrete case (1), we only sum the contributions to within the distance R. This introduces an error in the evaluation of the filtered function because the condition given by (4) does not apply. The error can be predetermined and set to a reasonably small value in the following manner. If one carries out the integration in (4) with respect to θ, the remaining integral can be rewritten as

$$\int_0^R \eta d(r^2/4K) + \int_R^{\infty} \eta d(r^2/4K) = 1. \quad (5)$$

Defining the second integral as ϵ yields

$$\int_0^R \exp(-r^2/4K)d(r^2/4K) = 1 - \epsilon, \quad (6)$$

where $\epsilon = \exp(-R^2/4K)$. In our analyses we have chosen $\epsilon = 0.02$, which implies with respect to (6) the representation of 98% of the influence of any data around the grid point in the area defined by the influence radius, R. In terms of the weight function used in the evaluation of (1) this choice leads to a value of $E = 4$ since $E = R^2/4K = -\ln \epsilon$. The choice of ϵ and the specification of R as a multiple of the average distance between grid points now determine the shape of the weight function.

Strictly speaking, the analysis applies only to areas of uniform data distribution. Our data distribution does not always meet this criterion. The choice of our first guess fields for different analysis periods was made to help alleviate the problem and will be discussed next.

The analysis scheme requires a first guess field that should be as realistic as possible. The method we used to obtain this first guess field was the same for each standard level and for all parameters. Thus, only the analyses of the temperature field will be discussed, but the same description applies to the analysis of all other parameters.

The first step was to compute an annual analysis. In this case, the first guess field was obtained by computing the zonal mean of the observed 1° square annual means for each 1° belt of latitude. Latitude belts that contained no observations were assigned values by linear interpolation from zonal means north and south of the missing belt or by extrapolation. The zonal mean of the 1° latitude belt was then used as the first guess value at each 1° square in that latitude belt. The final analysis of the annual mean then proceeded as described earlier.

The next step was to compute analyses for the Northern Hemisphere winter (December through May) and summer (June through November) semesters. Means for each 1° square for each semester were computed from the observed data. The first guess field used for these two analyses was the annual analysis. We then computed analyses for four 3-month seasons by using seasonal means computed from the observed data. The 3-month seasons were chosen so that the winter consisted of data from the months of February through April; spring, from May through July; summer, from August through October; and fall, from November through January. The first guess field for the winter and fall seasons was the 6-month winter analysis. The summer semester analysis was used as the first guess field for the summer and spring seasons. Finally, monthly analyses were computed from the observed monthly 1° square means with the appropriate 3-month seasonal analyses used as first guess fields. The MBT and XBT data were not available until we began the monthly analyses, so that the annual, semester, and seasonal analyses were based exclusively on the SD observations.

The advantage of the method just described can be illustrated as follows. If data were present in a region in only 1 of the 3 months of a particular season, then the analyses for the 2 months not containing data would generally be more realistic. This is generally the case

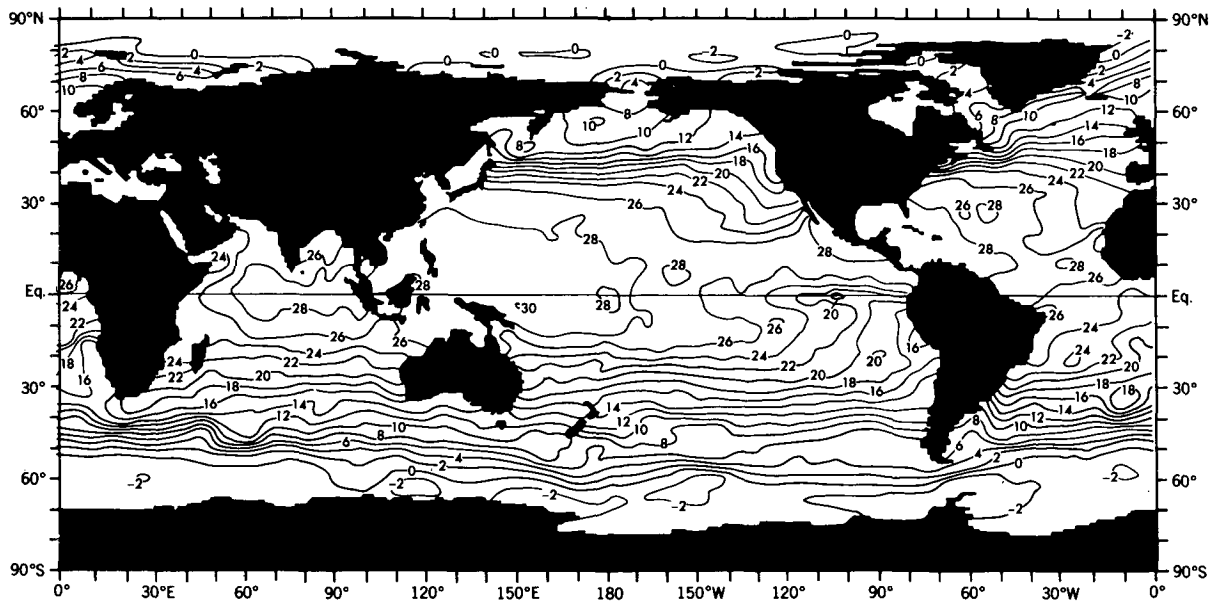

FIG. 10. Sea surface temperature analysis (in degrees Celsius) for the month of September.

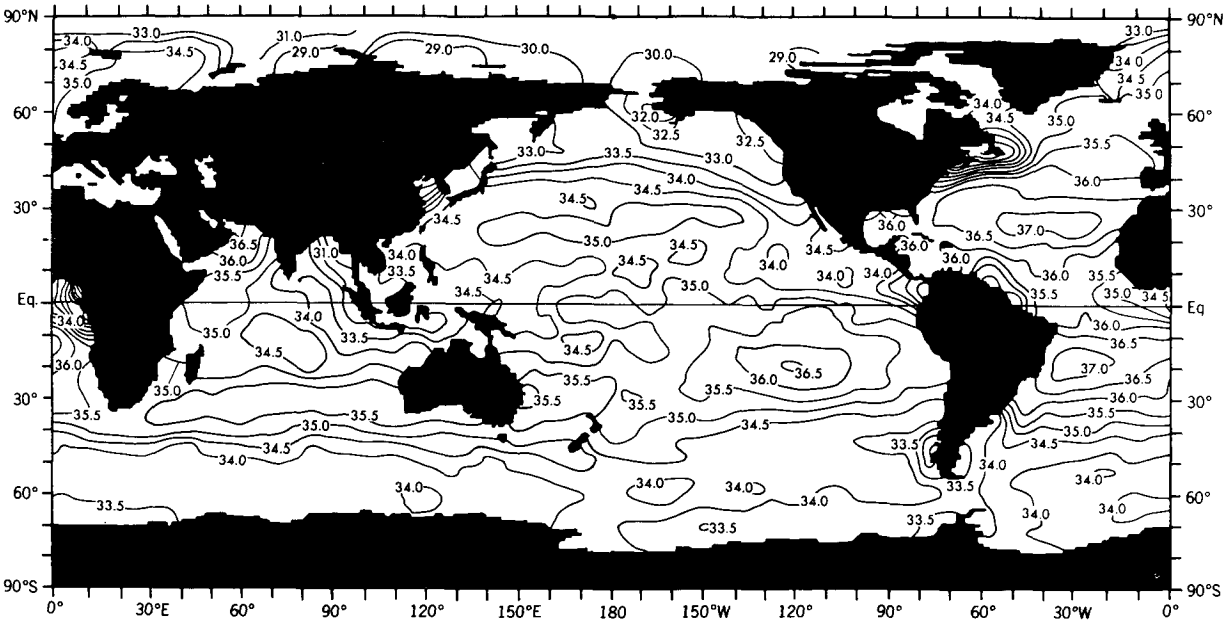

FIG. 11. Sea surface salinity analysis (in parts per mille) for the month of April.

because the first guess field will contain the influence of observations from the 1 month of the season containing data. However, an example in which this technique produces misleading results will be presented in the following section.

Annual, semester, seasonal, and monthly analyses were computed for salinity and temperature; annual, semester, and seasonal analyses for sigma-t; and an annual analysis for dissolved oxygen. The distribution of salinity observations does not fully justify monthly analyses for the world ocean, but they were computed for later use in certain areas of the Northern Hemisphere with sufficient data coverage.

6. Results

Some of our results are presented to give an overall impression of the project and to indicate some of the problems encountered. Other results are presented for comparison with previously published work in the literature. In particular, we chose to present the sea surface temperature for the month of September, which is shown in Fig. 10. This analysis can be compared in

part to results published in the *Oceanographic Atlas of the North Atlantic Ocean, Section 2, Physical Properties* (U.S. Naval Oceanographic Office, 1967). The sea surface analyses in the atlas were based on $>10^7$ merchant ship injection temperature reports that were averaged in 1° squares and then contoured. We chose not to include the merchant ship data in our analyses because we are interested in the three-dimensional structure of the ocean. Because the analyses in the atlas were computed from an independent data set consisting of considerably more observations than were used in our analyses, they represent a check on the representativeness of our data. Comparing the monthly analyses shows good agreement of the large-scale temperature distributions. A difference between the analyses is the distinctness of the warm northward-penetrating tongue of water associated with the Florida Current. The tongue is less distinct in our analysis and is associated with smoothing and the determination of the first guess field in our analysis scheme. Future work will attempt to remedy this situation.

The salinity analysis at the sea surface for the month of April is shown in Fig. 11. Some of the main features that appear are the subtropical salinity maximums. Furthermore, there is a distinct low salinity tongue in the Gulf of Panama, which is associated with an excess of precipitation over evaporation (Dietrich, 1957). Low salinity tongues associated with the runoff from the Amazon and Orinoco rivers are also present. Low surface salinities associated with runoff into the Arctic Ocean from rivers in Siberia and the Canadian Arctic appear but they are not real features for this month. This arises because the April data distribution for salinity (Fig. 8) shows that there were practically no observations present in the Arctic Ocean north of the Siberian and Canadian coasts because of the presence of ice. This implies that for this region our April analysis is simply the seasonal first guess field that was used. Examination of the distribution of salinity observations in this region for the other months of the year shows that only during July, August, and September are there significant numbers of observations available on which to base an analysis. Through first guess fields that remain unchanged because of the lack of observations, the summer data not only determine the annual analysis, but they also determine the analysis for each month. This implies that the low salinity tongues appearing in the Arctic result only from summer observations. This type of situation must be taken into consideration for the interpretation of our analyses in other data sparse areas as well. In polar regions, the situation can be rectified by using an ice cover distribution, such as that prepared by Alexander and Mobley (1976), to neglect ice-covered areas in computations if desired.

Vertical cross sections of temperature, salinity, and oxygen at 159.5°W are presented in Figs. 12a, 12b, and 12c, respectively. The temperature and salinity analyses of the upper 1 km represent the annual mean computed from the average of the 12 monthly analyses. The deeper (1–5 km) portions of these two sections and the oxygen section as a whole are annual analyses computed from all available data. These sections were chosen for comparison with similar sections presented by Reid (1965) as a check on our analysis scheme. The major features present are the tonguelike patterns in the oxygen and salinity sections that extend equatorward and downward

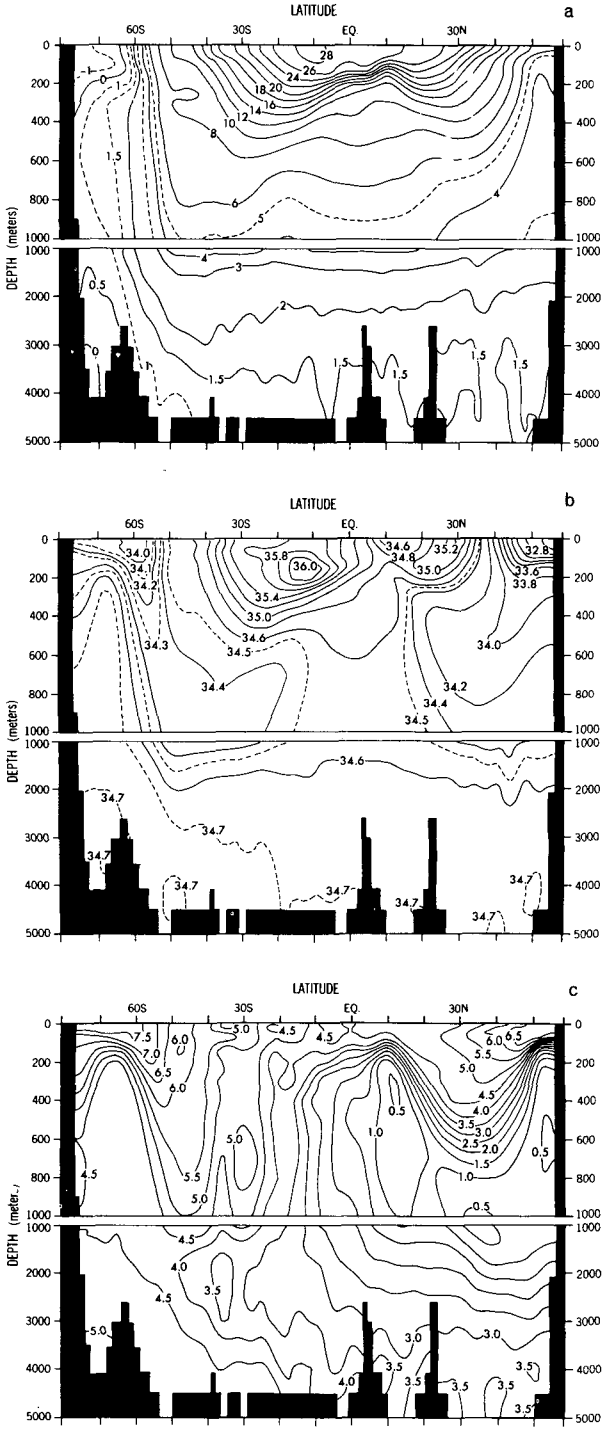

FIG. 12. Vertical cross section at 159.5°W of the annual mean (a) temperature (in degrees Celsius), (b) salinity (in per mille), and (c) oxygen (in milliliters per liter.)

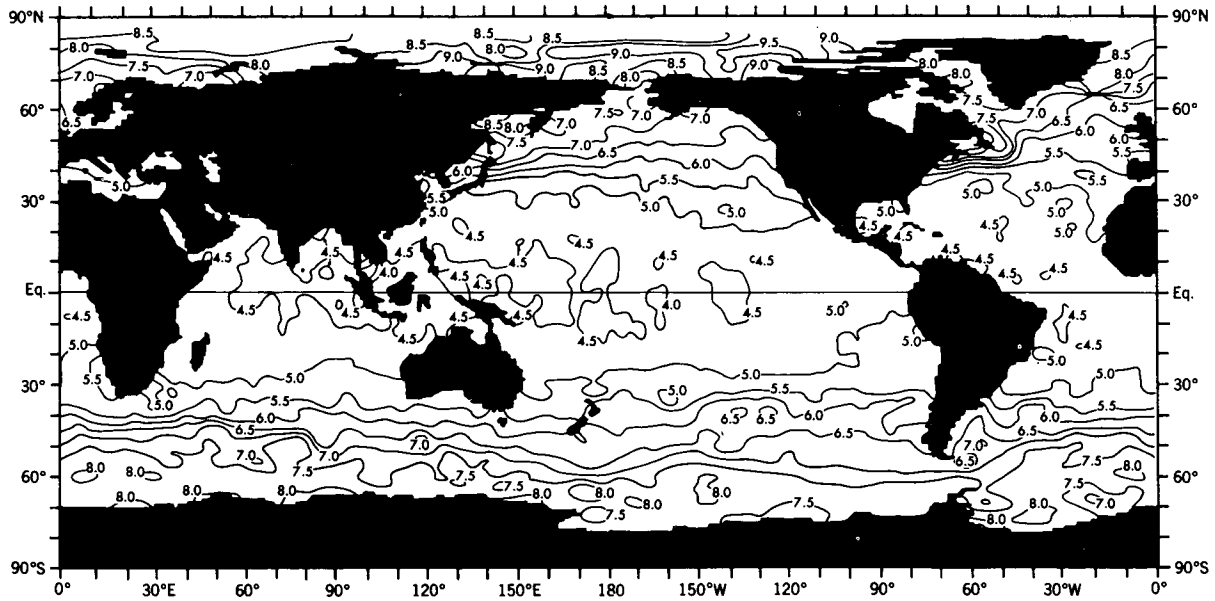

FIG. 13. Dissolved oxygen analysis (in milliliters per liter) at the sea surface for the annual period.

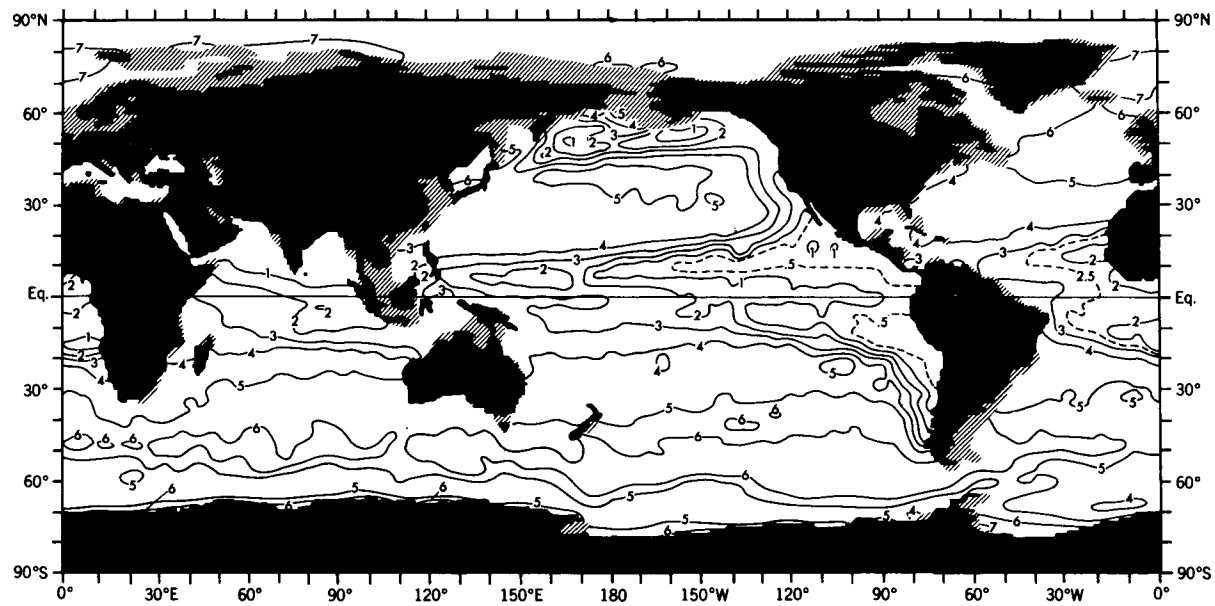

FIG. 14. Dissolved oxygen analysis (in milliliters per liter) at the 250 m level for the annual period.

from the surface at about 60°S and 55°N. The tongues represent intermediate water, and the processes governing their formation have been discussed by Reid. At 13°S and 23°N there are salinity maximums that represent subtropical water formed by the excess of evaporation over precipitation. Comparison of the sections in Fig. 12 with Figs. 2–4 of Reid (1965) shows generally good agreement, but there are some areas of disagreement. In Fig. 12a the equatorward bulge of the 8°C isotherm at 45°S and 250 m depth is probably in error, and in Fig. 12b the poleward bulge of the 35.6‰ isohaline at 28°S and 50 m depth is probably also in error. The deeper portions of Fig. 12 all show some disagreement with Reid's sections. In particular, the deep 1.5°C isotherm is disjointed, and the continuous deep Northern Hemisphere temperature minimum in Reid's section is not quite reproduced. These discrepancies are probably due to the quality control problems of the deep ocean that were discussed earlier.

The distribution of dissolved oxygen at the sea surface for the annual period is shown in Fig. 13. The global distribution of dissolved oxygen at the sea surface

closely parallels the surface distribution of temperature. This relationship is a result of two phenomena. First, the solubility of dissolved oxygen in seawater (Riley and Skirrow, 1975, p. 561) for the range of temperature and salinity that occurs in the open ocean is predominantly a function of temperature. Second, the amount of dissolved oxygen at the sea surface is generally near saturation (Richards, 1957). Comparing the results in Fig. 13 with the saturation values computed using our annual temperature and salinity analyses, we find that the surface distribution of oxygen shown is indeed near saturation.

The distribution of dissolved oxygen at a depth of 250 m in the world ocean is shown in Fig. 14. The distribution illustrates several features previously described by other researchers and summarized in a review article by Richards (1957). Some of the outstanding features of the distribution are the pairs of low oxygen tongues extending westward from the continents in the eastern Pacific and eastern Atlantic oceans at latitudes of ~10°N and ~10°S. Richards associated these minimums with upwelling that occurs in these regions. This idea is supported by a study by Defant (1961, p. 564) who used ship drift measurements to infer divergence and convergence in the surface current field in the world ocean. His results show horizontal divergence in the oxygen minimums regions, which does indicate upwelling. Richards also reviewed the importance of biological and chemical processes that affect the vertical distribution of oxygen. In brief, the upwelling in these regions brings relatively nutrient-rich, oxygen-poor water to the surface and this results in high organic productivity. The sinking of detritus in these regions leads to oxidative reduction and an increase in nutrients in the subsurface layers. Vertical profiles of oxygen in these regions show a strong minimum at depths of 500–600 m. Examination of the oxygen analyses at deeper levels shows that the tonguelike minimums are distinguishable at depths >1000 m. A complete understanding of the phenomena must include, among other factors, knowledge of the depth to which upwelling affects the water column, sinking rates of detritus, rate of oxidative reduction, diffusive effects, and advective effects.

Two centers of minimum oxygen on the 250 m map appear in the North Pacific Ocean at ~50°N. The distribution at this level indicates the great difference in circulation between the North Pacific and the North Atlantic Ocean. The North Atlantic contains no high-latitude minimums as the North Pacific does. This is undoubtedly due to the deep wintertime convection in the Norwegian and Greenland seas and in the Labrador Sea, which acts as a source of oxygen. Using the 5 ml/l isoline as a reference, we note that there appears to be a region of sinking or of mixing on isopycnal surfaces in the North Pacific centered approximately at 40°N, 165°W. The 250 m level is too deep for photosynthesis to be a source of oxygen.

If one compares the regions at the sea surface and 250 m with concentrations >5 ml/l, one can make the following observations. At the sea surface the regions meeting the criteria extend from the most poleward regions of the oceans to within ~30° of the equator in both hemispheres. This finding is consistent with the previous discussion concerning the factors governing the distribution of dissolved oxygen at the sea surface. At the 250 m level in the Arctic Ocean the region of high oxygen content is about the same as that at the surface. In the North Atlantic Ocean, the 5 ml/l isoline has retreated ~10° poleward from its position at the surface, whereas in the North Pacific Ocean, only a small region of high oxygen content remains. In the Southern Ocean a region

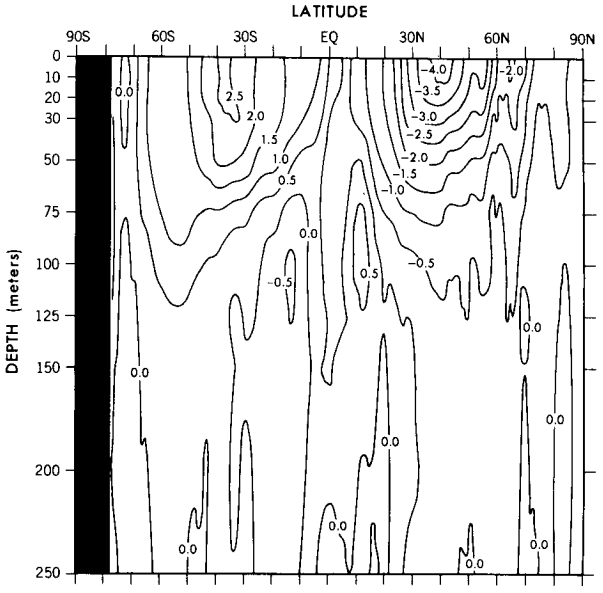

FIG. 15. Zonally averaged cross section of the March minus annual temperature difference field (in degrees Celsius).

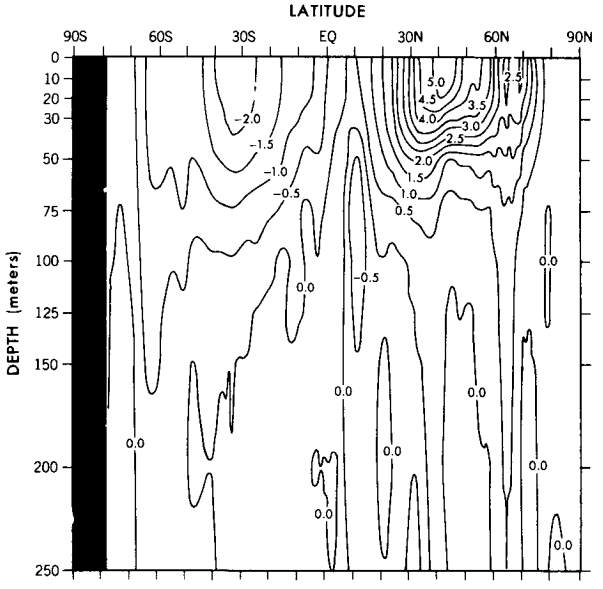

FIG. 16. Zonally averaged cross section of the September minus annual temperature difference field (in degrees Celsius).

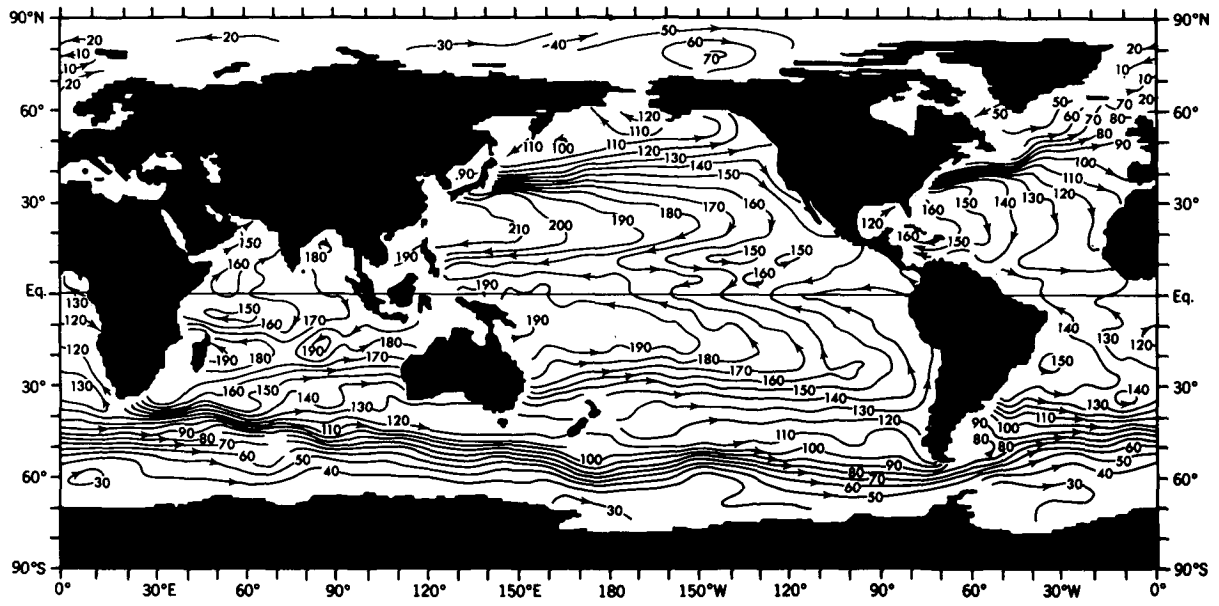

FIG. 17. Anomaly of geopotential height for the annual period (in dynamic centimeters).

higher than 5 ml/l at 250 m extends from ~33°S to within 15°–20° of latitude from the Antarctic coast. This southern boundary coincides with the mean position of the Antarctic convergence zone, and the oxygen distribution indicates sinking along the zone. There is a second region of high concentration that extends a few degrees seaward from the Antarctic coast.

Vertical cross sections of the zonally averaged March and September temperature fields minus the zonally averaged annual mean field from the surface to a depth of 250 m are presented in Figs. 15 and 16. March and September were chosen because they represent the months when extremes in sea surface temperature are found in mid-latitudes. The figures can be interpreted only in a general way since they represent zonal averages over all ocean basins. Maximum temperature differences occur at latitudes of ~35°S and ~40°N. The depth of penetration of the annual wave as determined by the depth of the ±0.5°C isolines is ~100 m. Below this level, it was found from distributions of other months (not presented here) that there is approximately a 2-month lag between the extremes found at the surface and the extremes found at these deeper levels.

As a final item of possible interest, a map of the mean annual anomaly of geopotential height is shown in Fig. 17. The computation is presented only for those ocean areas with depths >1000 m because the large nearshore gradients present contouring difficulties. The density fields used to compute the geopotential were computed from the annual average of the monthly temperature and salinity fields. The approximation of substituting depth in meters for pressure in decibars was made. The main features shown in Fig. 17 are the anticyclonic flows associated with the subtropical gyres, the cyclonic flows in the North Pacific and North Atlantic, the eastward flow of the Antarctic Circumpolar Current, and the ridge-trough system associated with equatorial flow, which appears in all of the oceans. Figure 17 may be compared to a global map of geopotential anomaly presented by Stommel (1964). Stommel's map is a composite of maps for individual oceans prepared by several different authors. The overall agreement between Fig. 17 and Stommel's map is good. For the Pacific Ocean, Fig. 17 can be compared with a map of the mean annual anomaly geopotential height for the Pacific Ocean presented by Wyrtki (1975), which is based on a more recent data base than Stommel's map. The large-scale features of both maps are in good agreement although we do not find in our annual analyses the relative extremes in either the Gulf of Panama or the region south of Japan that Wyrtki found. However, we find these extremes in our monthly analyses.

7. Future work

We have obtained an additional 190 000 XBT stations, 70 000 MBT stations, and 80 000 SD observations from NODC, which update our files through June of 1976. These data will be merged with the data set used to compute the fields shown in this paper. New analyses will be computed based on the enlarged data set, with refinements in the analysis scheme and with the elimination of certain errors in the data that escaped our earlier quality control.

In the near future we intend to produce an atlas containing standard level analyses and zonal cross sections for the globe and individual oceans. In addition, the standard level analyses may be made available, possibly through a national data center if there appears to be sufficient interest in the scientific community.

Acknowledgments. The authors would like to thank Greg Tripoli who programed the original objective analysis scheme and made helpful suggestions. In addition we would like to thank Jim Welsh whose suggestions and guidance were invaluable in unpacking the data used in this study and for programing suggestions in general. Tom Reed provided valuable programing suggestions with regard to computer plotting of the analyses. Thanks also go to Kirk Bryan and Alan Blumberg for their comments on the manuscript and to Betty Williams, John Conner, and Phil Tunison and his co-workers for help in preparation of the manuscript.

References

Alexander, R. C., and R. L. Mobley, 1976: Monthly average sea-surface temperatures and ice-pack limits on a 1° global grid. *Mon. Wea. Rev.*, **104**, 143–148.

Barnes, S. L., 1963: A technique for maximizing details in numerical weather map analysis. Atmospheric Research Lab., Univ. of Oklahoma Research Institute, Norman. (Unpublished report.)

Bergthörsson, P., and B. Döös, 1955: Numerical weather map analysis. *Tellus*, **7**, 329–340.

Cressman, G. P., 1959: An operational objective analysis scheme. *Mon. Wea. Rev.*, **87**, 367–374.

Defant, A., 1961: *Physical Oceanography*. Vol. 1., Pergamon, New York, 729 pp.

Dietrich, G., 1957: *General Oceanography*. Interscience, New York, 588 pp.

Ellis, J. S., T. H. Vonder Haar, S. Levitus, and A. H. Oort, 1977: The annual variation in the global heat balance of the earth. *J. Geophys. Res.*, **82**, in press.

NOAA, 1974: *User's Guide to NODC's Data Services*. Environmental Data Service, Washington, D.C.

Oort, A. H., and T. H. Vonder Haar, 1976: On the observed annual cycle in the ocean-atmosphere heat balance over the Northern Hemisphere. *J. Phys. Oceanogr.*, **6**, 781–800.

Reid, J. L., 1965: *Intermediate Waters of the Pacific Ocean. Johns Hopkins Oceanogr. Stud.*, Johns Hopkins Press, Baltimore, 85 pp.

Richards, F. A., 1957: Oxygen in the ocean. *Mem. Geol. Soc. Amer.*, **67**, 185–238.

Riley, J. P., and G. Skirrow, 1975: *Chemical Oceanography*. Vol. 1, Academic, New York, 606 pp.

Sasaki, Y., 1960: An objective analysis for determining initial conditions for the primitive equations. Ref. 60-16T, Atmospheric Research Lab., Univ. of Oklahoma Research Institute, Norman, 22 pp.

Smith, S. M., H. W. Menard, and G. Sharman, 1966: Worldwide ocean depths and continental elevations. SIO Ref. G5-8, Scripps Institution of Oceanography, Univ. of California, La Jolla, 17 pp.

Stommel, H., 1964: Summary charts of the mean dynamic topography and current field at the surface of the ocean, and related functions of the mean wind-stress. *Studies on Oceanography*, edited by K. Yoshida, University of Tokyo Press, Tokyo, pp. 53–58.

U.S. Naval Oceanographic Office, 1967: *Oceanographic Atlas of the North Atlantic Ocean, Section 2: Physical Properties*. H. O. Pub. 700, Washington, D.C., 300 pp.

Wyrtki, K., 1975: Fluctuations of the dynamic topography in the Pacific Ocean. *J. Phys. Oceanogr.*, **5**, 450–459. •

announcements

U.S. Climate Program Plan

Copies of the 79-page booklet, "A United States Climate Program Plan," are now available to the public. The plan was prepared by a drafting group from the Interdepartmental Committee for Atmospheric Sciences (ICAS). Copies may be requested from: National Climate Program Coordinating Office, Dept. of Commerce, NOAA, WSC-5, 6010 Executive Blvd., Rockville, Md. 20852.

CIRES fellowships

The Cooperative Institute for Research in Environmental Sciences (CIRES) offers one year Visiting Fellowships to scientists with research interests in the areas of atmospheric science, solid earth science, atmospheric and terrestrial EM wave propagation, and paleo and rock magnetism. Recipients of these awards are completely free to pursue their own research programs. Selection is made on the likelihood of an active exchange of ideas between the Visiting Fellow and the scientists in CIRES and other local research groups. Stipend is scaled to research experience, and the program is open to scientists of all countries.

Applications for the 1978–79 academic year awards should be received before *1 February 1978* and should include a curriculum vitae, publications list, the names of three professional references, and a brief outline of the intended research. CIRES is jointly sponsored by the University of Colorado and the NOAA Environmental Research Laboratories. For further information, contact: The Director, Visiting Fellows Program, CIRES, University of Colorado, Boulder, Colo. 80309.

Continued on page 1296